

Manipulating the electron dynamics in the non-sequential double ionization process of Ar atoms by an orthogonal two-color laser field

Pengzhao Wang(王鹏昭), Lijie Qian(钱丽洁), Zhenrong Sun(孙真荣), and Yan Yang(杨岩)

Citation: Chin. Phys. B, 2024, 33 (**6**): 063201. DOI: 10.1088/1674-1056/ad2606
Journal homepage: http://cpb.iphy.ac.cn; http://iopscience.iop.org/cpb

What follows is a list of articles you may be interested in

Multiple collisions in crystal high-order harmonic generation

Dong Tang(唐栋) and Xue-Bin Bian(卞学滨)
Chin. Phys. B, 2022, 31 (**12**): 123202. DOI: 10.1088/1674-1056/ac6b2c

Imprint of transient electron localization in H_2^+ using circularly-polarized laser pulse

Jianghua Luo(罗江华), Jun Li(李军), and Huafeng Zhang(张华峰)
Chin. Phys. B, 2020, 29 (**12**): 123201. DOI: 10.1088/1674-1056/abbbe1

Bohmian trajectory perspective on strong field atomic processes

Xuan-Yang Lai(赖炫扬), Xiao-Jun Liu(柳晓军)
Chin. Phys. B, 2020, 29 (**1**): 013205. DOI: 10.1088/1674-1056/ab5c0f

Exploration of strong-field double ionization of C_3H_6 with the structures of propene and cyclopropane in intense laser fields

Qing-Yun Xu(徐清芸), Yan-Rong Tian(田艳荣), Hui-Zhong Lu(卢惠中), Jun Zhang(张军), Tong-Tong Xu(徐彤彤), Hong-Dan Zhang(张宏丹), Xue-Shen Liu(刘学深), Jing Guo(郭静)
Chin. Phys. B, 2018, 27 (**3**): 033202. DOI: 10.1088/1674-1056/27/3/033202

Theoretical study on non-sequential double ionization of carbon disulfide with different bond lengths in linearly polarized laser fields

Kai-Li Song(宋凯莉), Wei-Wei Yu(于伟威), Shuai Ben(贲帅), Tong-Tong Xu(徐彤彤), Hong-Dan Zhang(张宏丹), Pei-Ying Guo(郭培莹), Jing Guo(郭静)
Chin. Phys. B, 2017, 26 (**2**): 023204. DOI: 10.1088/1674-1056/26/2/023204

Manipulating the electron dynamics in the non-sequential double ionization process of Ar atoms by an orthogonal two-color laser field

Pengzhao Wang(王鹏昭)[1], Lijie Qian(钱丽洁)[1], Zhenrong Sun(孙真荣)[1,2,†], and Yan Yang(杨岩)[1,‡]

[1] *State Key Laboratory of Precision Spectroscopy, East China Normal University, Shanghai* 200241, *China*
[2] *Collaborative Innovation Center of Extreme Optics, Shanxi University, Taiyuan* 030006, *China*

(Received 27 December 2023; revised manuscript received 24 January 2024; accepted manuscript online 5 February 2024)

Electron dynamics during non-sequential double ionization (NSDI) is one of the most attractive areas of research in the field of laser–atom or laser–molecule interaction. Based on the classic two-dimensional model, we study the process of NSDI of argon atoms driven by a few-cycle orthogonal two-color laser field composed of 800 nm and 400 nm laser pulses. By changing the relative phase of the two laser pulses, a localized enhancement of NSDI yield is observed at 0.5π and 1.5π, which could be attributed to a rapid and substantial increase in the number of electrons returning to the parent ion within extremely short time intervals at these specific phases. Through the analysis of the electron–electron momentum correlations within different time windows of NSDI events and the angular distributions of emitted electrons in different channels, we observe a more pronounced electron–electron correlation phenomenon in the recollision-induced ionization (RII) channel. This is attributed to the shorter delay time in the RII channel.

Keywords: non-sequential double ionization, electron dynamics, few-cycle orthogonal two-color laser field

PACS: 32.80.Fb, 33.20.Xx, 33.80.Eh, 34.50.Rk **DOI:** 10.1088/1674-1056/ad2606

1. Introduction

With the rapid development of ultrafast laser technology,[1] it is possible to effectively and precisely observe and measure the ultrafast dynamics of light–atom (or light–molecule) interactions on femtosecond or even attosecond time scales. This has led to significant breakthroughs in various fields such as chemical reaction control,[2] high-order harmonic generation,[3] real-time observation of electronic dynamics[4,5] and other disciplines. Among these achievements, not only the unique quantum effect of the electron itself but also the mysterious electron–nuclei and electron–electron coupling during ionization dynamics have attracted much attention.[6–8] When an atom or molecule is exposed to a sufficiently strong external electric field, for example, a laser field, its electrons can be ionized by various mechanisms, including multiphoton ionization, above-threshold ionization and tunneling ionization. If two electrons are ionized one by one, this process is referred to as sequential double ionization (SDI). In other words, these two ionization events are independent and occur in sequence. In contrast, in non-sequential double ionization (NSDI), two electrons are ejected from the atom or molecule within a short time interval. After the first electron is ejected, it is driven back to the parent ion by the oscillating external field and collides with the parent ion. It can transfer some or all of its kinetic energy to the second electron,[3] leading to the process of direct ionization (recollision-induced ionization, RII) or ionization after optical excitation (RESI)[6] of the second electron.

Compared with the simple SDI process, the NSDI process involves complex multi-body interactions, especially the 'recollision' mechanism, which lead to more rich and complex dynamics of electrons in a single optical period.[3] This provides an ideal model for studying and understanding electron–electron and electron–parent ion correlation effects. In the last two decades, a variety of theoretical and experimental methods have been used to explore electron energy correlations,[9,10] angular distribution correlations,[11] and recollision processes[12,13] in NSDI. Considering that electronic dynamics occurs on attosecond time scales, and the released electron trajectories are mainly manipulated by changing the laser field parameters, many researchers have utilized pulse-shaping[14–19] or multi-color laser fields[20–24] to study the NSDI process. In particular, an orthogonal two-color (OTC) laser field, in which two laser beams with different frequencies are orthogonally polarized in space, has been widely used to control the electron dynamics.[25,26] The unique asymmetry created by the spatially orthogonal field components can guide electron trajectories and pave the way for complex electron and ion manipulations. Zhou *et al.* studied NSDI of He atoms in a classical model using parallel and orthogonal two-color laser fields.[27,28] They observed a narrow circular distribution of correlated electronic momentum and were able to control the correlation and anti-correlation behavior of electronic momentum along the direction of polarization of the laser by controlling the relative phase of the two laser beams; they achieved attosecond precision control of the electronic

†Corresponding author. E-mail: zrsun@phy.ecnu.edu.cn
‡Corresponding author. E-mail: yyang@lps.ecnu.edu.cn

© 2024 Chinese Physical Society and IOP Publishing Ltd

recollision time. Li *et al.* studied NSDI of Ar atoms using OTC laser fields with different wavelength combinations in the classical ensemble model, and found that changing the laser frequency in the OTC laser field can control the electron return probability and the direction of momentum of the doubly charged ions.[29] Gong *et al.* used phase-controlled OTC laser pulses to study the time delay of photoelectron emission in strong-field ionization of Ar atoms. By controlling the relative phase, they were able to clearly distinguish the main peak and sideband peaks in the above-threshold ionization spectrum.[30] Xie *et al.* utilized an OTC laser field to separate the quantum pathways in multiphoton ionization of Ar atoms, and discovered interference in the momentum distribution of photoelectrons caused by nonadjacent quarter cycles of the quantum pathways.[31]

In the realm of experimental physics, the generation of a few-cycle OTC laser field is a major challenge. The inherent complexity and technical limitations make it particularly difficult to perform time-resolved, high-precision measurements related to electronic dynamics. Therefore, theoretical calculations are an indispensable avenue that provides physicists with valuable insights and a deeper understanding of the underlying processes. People have extensively studied NSDI using classical theoretical models; these are based on aspects such as yield modulation, momentum distribution at specific moments and classical trajectories, yet lack continuous dynamic observation of the behavior of two correlated electronic dynamics over a period of time. This paper uses a classical ensemble model to study the NSDI of Ar atoms driven by a few-cycle OTC laser field. This indicates that the NSDI yield is regulated by the relative phase of two laser pulses. We present an approach that analyzes the electron–electron momentum correlation during NSDI moments within different time windows, as well as the angular distribution of emitted electrons in various channels. It has been discerned that the electron–electron correlation phenomenon in the RII channel is more pronounced due to the shorter delay time for recollision events.

2. Method and model

In this paper, a fully classical treatment of the two-electron systems proposed by Wang *et al.*[32] has been performed to calculate the electron trajectory, electron–electron correlation and recollision dynamics during NSDI of Ar atoms. A detailed description is given in Ref. [33]. Briefly, the electrons are restricted in a two-dimensional (2D) plane, and the Hamiltonian of the two active electrons can be written as (atomic units are used throughout unless otherwise specified)

$$H_{\mathrm{e}} = \sum_{i=1,2}\left[\frac{p_i^2}{2} - \frac{2}{\sqrt{r_i^2+a^2}}\right] + \frac{1}{\sqrt{r_{12}^2+b^2}}, \tag{1}$$

where r_i and p_i represent the position and momentum of the ith electron, respectively, and r_{12} is the distance between the two electrons. To avoid autoionization and computational singularity, the soft-core Coulomb potential is used, where a and b are smoothing parameters.[34] For the ensemble with Ar atoms, a is set to 1.5 and b is set to 0.1. The motion of two electrons in the x–y plane is determined by the following canonical equation:[35]

$$\frac{\mathrm{d}r_i}{\mathrm{d}t} = \frac{\partial H_{\mathrm{e}}}{\partial p_i}, \quad \frac{\mathrm{d}p_i}{\mathrm{d}t} = -\frac{\partial H_{\mathrm{e}}}{\partial r_i}. \tag{2}$$

This equation can be solved using the standard fourth-order Runge–Kutta algorithm. The ensemble (e.g., 10^6 Ar atoms) is initially populated by randomly placing the electrons in the position and momentum spaces. Once the position of each pair of electrons has been randomly assigned, the corresponding residual energy is determined. Then the ensemble is allowed to evolve for a sufficiently long time (normally over 150 a.u.) without fields, then the stable distribution of the electrons in position and momentum spaces can be obtained. As long as the total energy of the two electrons in the ensemble is confirmed, a butterfly-like stable distribution in both spaces can be observed. When the laser field is turned on, the system Hamiltonian is given by

$$H = H_{\mathrm{e}} + (r_1 + r_2)\cdot E(t), \tag{3}$$

and the total electric field of the two-color laser pulse $E(t)$ can be written as

$$E(t) = E_0\left[f_x(t)\cos(\omega t)e_x + \beta f_y(t)\cos(2\omega t + \Delta\Phi)e_y\right], \tag{4}$$

where $f(t)$ is the pulse envelope (e.g., Gaussian shape), E_0 and ω represent the amplitude and frequency of the 800 nm fundamental laser field, respectively, β is the intensity ratio of the electric field of the two-color components, $\Delta\Phi$ is the relative phase between the two-color laser fields and x and y denote the polarization vector directions of 800 nm and 400 nm laser fields, respectively. The pulse durations (FWHM) of the fundamental and second-harmonic pulse are both 10 fs and the focal volume effect is not considered here.

During the calculation we can record the information on the positions (x, y), momenta (p_x, p_y), kinetic energy release (KER) and total energy of every electron at each step (with a time interval of 0.2 a.u.). With this recorded information, we can establish several definitions. When the energy of an electron exceeds zero it means that this electron has ionized, and this moment is defined as t_1. After experiencing the oscillation of the OTC field, this electron returns to the parent ion. When the Coulomb repulsion between electrons reaches a maximum, it means that a recollision event has occurred and the energy of the electrons has been exchanged. The recollision time (t_{re})

is defined as the instant when the repulsion energy of the two electrons reaches its maximum for the first time after the first ionization event. The second electron undergoes ionization after receiving a portion of energy from the first electron, or it may be excited and subsequently ionized in the following laser field. The final double ionization time ($t_{\rm DI}$) is defined as the instant when the energies of the two electrons are both positive (including the kinetic energy and the potential energy). Among all the double ionization events, the events that have had electron recollision and for which the recollision time is earlier than the double ionization time are screened out, i.e., NSDI events (i.e., $t_{\rm DI} > t_{\rm re}$). In this case, the time of NSDI is proven to be the double ionization time (i.e., $t_{\rm NSDI} = t_{\rm DI}$). The travel time is defined as $t_{\rm travel} = t_{\rm re} - t_1$. The delay time is defined as $t_{\rm delay} = t_{\rm NSDI} - t_{\rm re}$. The optical cycle is 2.67 fs, while the reference time zero point is designated as the moment 600 a.u. ($\sim$ 14.51 fs) prior to the peak of the electric field of an 800 nm laser field. These definitions are adopted in this paper and will not be reiterated in subsequent sections.

3. Results and discussion

3.1. Optimizing the yield of NSDI

In a certain laser intensity range, the double ionization yield no longer increases with increase in the laser power. This 'knee'-like structure.[36,37] is regarded as an important symbol of the NSDI phenomenon. In other words, NSDI only takes place in a certain laser intensity range. Beyond this range, the double ionization yield is very low or SDI dominates the double ionization process. Therefore, the vector sum of the electric field intensities of the fundamental and second harmonic fields is chosen within the range 0.2–0.8 PW·cm^{-2}. Figure 1 compares the yield (normalized to the maximum value of 0.8 PW· cm^{-2}) of NSDI events at different relative phases of the OTC laser field. The corresponding relative phases of maximum yield of NSDI events for each laser intensity are about 0.125π and 1.125π, and the relative phases of minimum yield are about 0.75π and 1.75π. The yield curve shows cyclic trends and changes with the relative phase. This indicates that the NSDI yield rates are strongly influenced by the relative phase. In particular, there is a small hump around the relative phases of 0.5π and 1.5π at a laser intensity of 0.2 PW·cm^{-2}. This is very interesting and will be discussed in the following text. It is known that the key point in the NSDI process is recollision, which not only directly determines the yield of NSDI events but also drives the energy correlation between electrons. Therefore, the statistical distribution of the rate of recollision events at different recollision times within three to eight cycles is shown in Fig. 2. The top and bottom rows show the statistics for recollision time at 0.125π and 0.75π for different laser intensities. It can be seen that the number of recollision events is much lower at a relative phase of 0.75π than at 0.125π. This means that the OTC laser field can effectively control the recollision process of the first electron by changing the relative phase. Moreover, the difference in the number of recollision electrons leads directly to a change in the yield of NSDI events, which can explain the modulation of the yield by different relative phases. In addition, some other interesting information can be gleaned from Fig. 2. For 0.125π, the distribution of the recollision time is spread over a relatively wide range of optical cycles (almost four cycles) and shifts to an earlier time as the laser intensity increases. In contrast, the distribution at 0.75π is much narrower than that at 0.125π, and 75%–87% of the recollision events gradually concentrate in the range of three to five cycles with increasing laser intensity. In other words, by adjusting the relative phase and laser intensity of the OTC laser field, the recollision time on the attosecond scale and the number of recollision events can be manipulated.

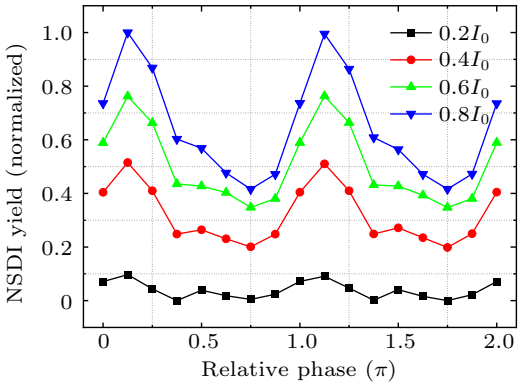


Fig. 1. Yield of NSDI events as a function of the relative phase at four different laser field intensities ($I_0 = 1$ PW·cm^{-2}). The yield is normalized to the maximum yield of $0.8I_0$.

3.2. Travel time of the first electron

The travel time ($t_{\rm travel}$) is a critical parameter for manipulating NSDI dynamics in an OTC laser field. The relationship between the number of recollision electrons, $t_{\rm travel}$, and the relative phase is shown in Fig. 3. As the laser intensity increases, the number of NSDI events increases significantly, which is consistent with the trend in Fig. 1. For different laser intensities, all spectra show similar distributions, where the rate of production of NSDI events shows a periodic variation trend along with the travel time and relative phase changes, and decreases with increasing travel time. When the relative phase is 0.5π–0.75π (1.5π–1.75π), most of the events are concentrated within less than 0.2 cycles of the travel time, indicating that the electron recollides with the parent nuclei immediately after the first ionization. In other relative phases, the travel time is mainly concentrated in the range 0.4–0.7 cycles.

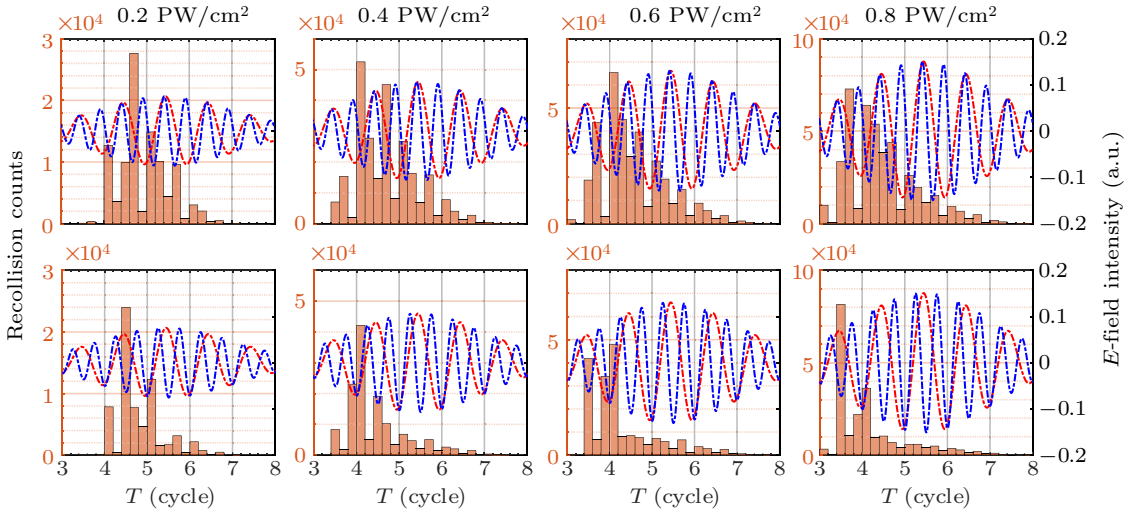


Fig. 2. The statistical distribution of recollision event rates at different recollision times under two typical relative phases: 0.125π (upper row) and 0.75π (bottom row) at four different laser field intensities.

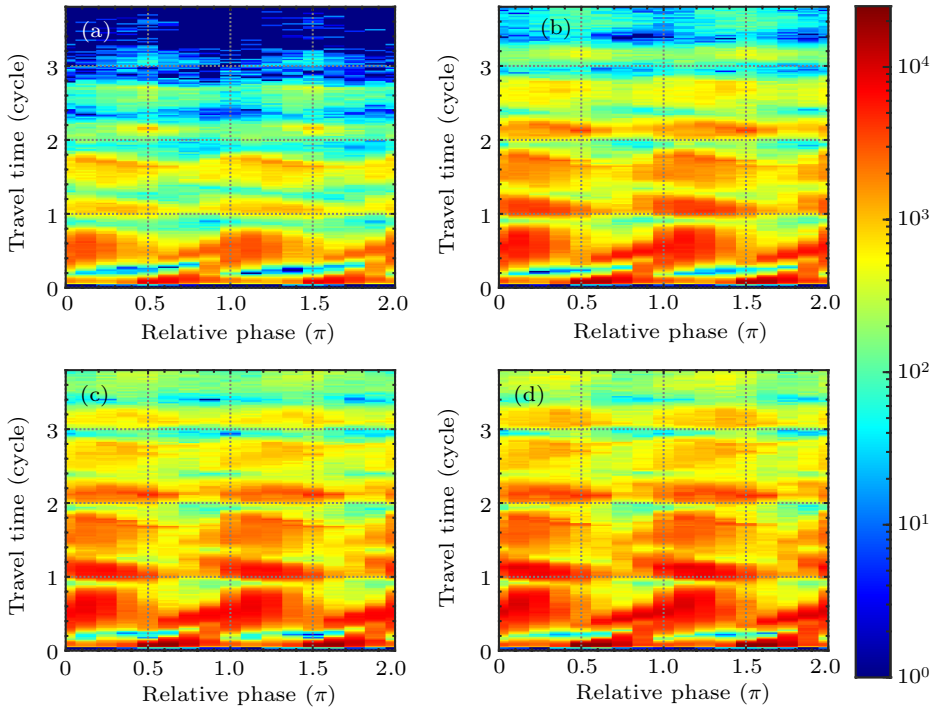


Fig. 3. The relationship between the number of recollision electrons, t_{travel} and relative phase. Laser field intensities are (a) 0.2 PW·cm^{-2}, (b) 0.4 PW·cm^{-2}, (c) 0.6 PW·cm^{-2}, (d) 0.8 PW·cm^{-2}. The color bar represents the number of recollision electrons.

3.3. KER of the first electron

According to the rescattering model, in an OTC field the KER of the first ionized electron can also be effectively controlled by the relative phase. In Figs. 4(a)–4(c), the KERs of the first ionized electrons with different t_{travel} in different relative phases are plotted. The vast majority of electrons have a large KER (> 0.5 a.u.) and sufficient energy to transfer to the second electrons upon recollision with the parent ion. Since all statistical events are assigned to events where the NSDI phenomenon occurred, the sum of the probabilities of the different t_{travel} events in Fig. 4(d) directly corresponds to the yield of NSDI events in three relative phases. The integration of the probability for the three relative phases (0.125π, 0.5π and 0.75π) is 0.22, 0.17 and 0.14, respectively. For 0.125π (the black line), t_{travel} is mainly distributed in a wide range from 0.4 to 0.7 cycles. Compared with the other two relative phases, the largest integration value represents the highest yield of NSDI events. For 0.75π (the blue line), t_{travel} has two main distribution ranges, 0.06–0.28 cycles and 0.38–0.64 cycles, but due to its small integral area, the corresponding yield of NSDI events is relatively low. The above situations are consistent with the NSDI trend of 0.2 PW·cm^{-2} in Fig. 1. However, for 0.5π (the red line), a large fraction of t_{travel} ($> 50\%$) is concentrated in the very narrow range from 0.06 to 0.16 cycles, indicating a substantial increase in the number of electrons returning to the

parent ions in a very short time. The shortening of travel time increases the likelihood of multiple collisions between electrons and parent ions, while the high energy carried by these electrons further facilitates the ionization of secondary electrons, thereby enhancing the yield of NSDI. Therefore, the hump shown in Fig. 1 (at 0.5π) can be explained reasonably.

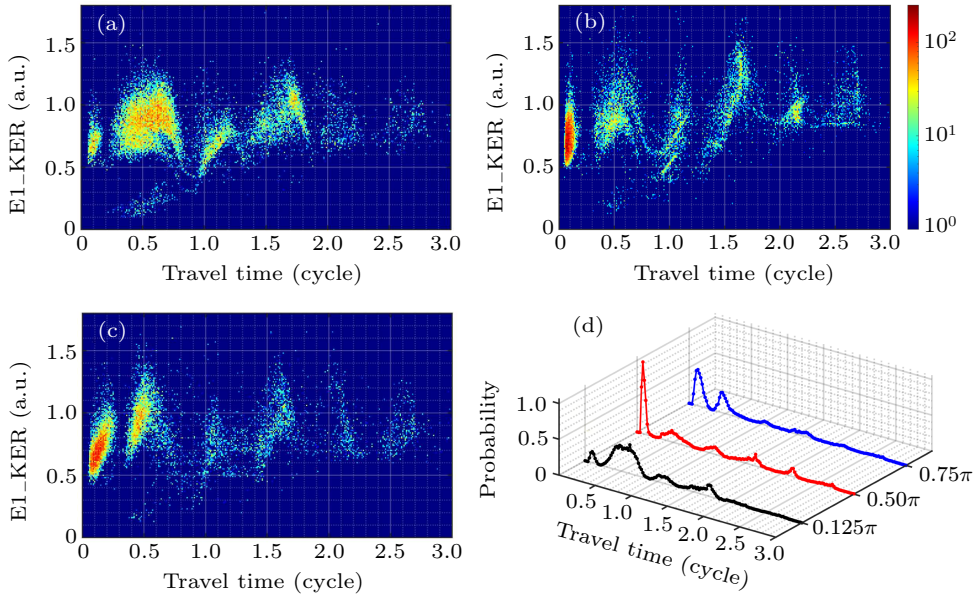


Fig. 4. The maximum KER of the first electron as a function of travel time is depicted for three characteristic relative phases, (a) 0.125π, (b) 0.5π and (c) 0.75π, all under a laser electric field intensity of 0.2 PW·cm^{-2}. (d) Probability statistics for various travel times under the aforementioned relative phases, with probabilities normalized to the peak value at 0.5π.

3.4. Double ionization mechanism

After the first electron recollides with the parent ion, direct (RII) or indirect (RESI) ionization of the second electron will be triggered. This process can be clearly seen in Fig. 5. Figure 5(a) shows the 2D statistics of the energy distribution of the doubly ionized electrons as a function of time evolution. The electron energy oscillates in a range from -0.78 to -0.02 a.u. before the third cycle. Between the third and the fourth cycles, the distribution splits into two branches. One of them enters the positive energy region while the other drops to a lower negative energy region, which means that just single ionization occurs. Then the ionized electron returns to the parent ion (the energy becomes negative) and collides with the second electron, which corresponds to a recollision process. After the seventh optical cycle, the energy distribution is essentially in the positive energy region, indicating that the vast majority of Ar atoms have completed double ionization. In Figs. 5(b)–5(d), the blue line represents the repulsion energy between the first and second electrons. When the repulsion energy reaches a maximum after the first electron is ionized it means that the first electron recollides with the parent ion. The red and black lines represent the energy profile of the first and second electrons, respectively. Figure 5(b) shows a typical RII channel, where the first ionized electron returns to the nucleus and collides with the second electron, whereupon the two electrons are immediately ionized. The last two figures show two different RESI channels. In Fig. 5(c), the first electron transfers less energy to the second electron when it collides with the parent ion and then escapes from the parent ion again. The second electron is populated to the excited state and will be ionized in the subsequent laser field. In Fig. 5(d), when the first electron collides with the parent ion too much energy is transferred to the second electron, which is ionized directly, so it is recaptured by the parent ion and populated to the excited states. Similar to Fig. 5(c), this electron will be ionized in the subsequent laser field after gaining enough energy.

The time difference (t_{delay}) between the moment of double ionization and the moment of recollision is an important indicator for distinguishing the two NSDI processes mentioned above. However, there is no unified and widely accepted time delay value that can be used for its determination. In this work, the RII channel is defined as an ionization process with a delay time of less than 0.2 cycles. Accordingly, those with a longer delay time are classified as the RESI channel. This classification standard will also be used in the rest of the discussion. The OTC laser field not only provides the driving energy for the non-sequential double ionization of Ar atoms, but also has various controlling effects on the emitted electrons with different relative phases. Once the assignment of NSDI events is completed, it is natural to analyze the manipulation of the OTC laser field to the two NSDI channels. Figure 6 presents the ratios $N/(N_{\text{RII}}+N_{\text{RESI}})$, where N is the yield of the corresponding channel, as a function of the different relative phases at an intensity of 0.6 PW·cm^{-2} with each curve normalized separately. It can be seen from the figure that the yield of the two channels shows a completely opposite trend, which indirectly confirms the rationality of using a delay time of 0.2 cycles to distinguish between RII and RESI channels. When the relative phases are 0.375π and 1.375π, the RII channel

achieves the maximum yield while the RESI channel has the minimum yield. When the relative phase shifts from 0.375π to 0.75π or 1.375π to 1.75π, the extreme points of the yield curves of the two channels reverse compared with the previous relative phase. The yield of the two channels is strongly regulated by the relative phase, which provides an effective way to coherently control the electron dynamics on an attosecond time scale.

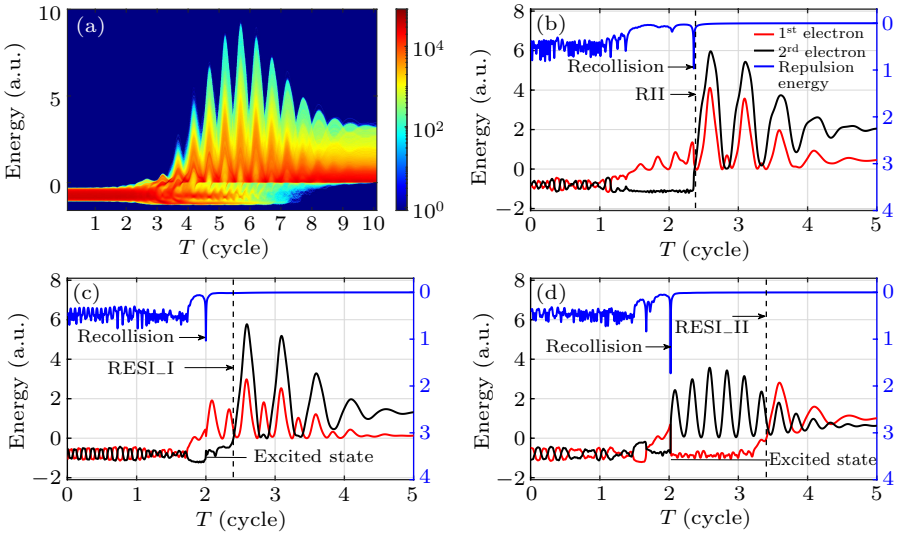


Fig. 5. (a) Time evolution of the total energy of the two electrons individually. (b)–(d) Three typical energy evolution processes of the NSDI mechanism. The laser intensity is 0.6 PW·cm^{-2}. The legend in (b) is uniformly used in (b)–(d). The red line represents the energy of the first electron, the black line represents the energy of the second electron and the blue line represents the Coulomb repulsion force between the two electrons.

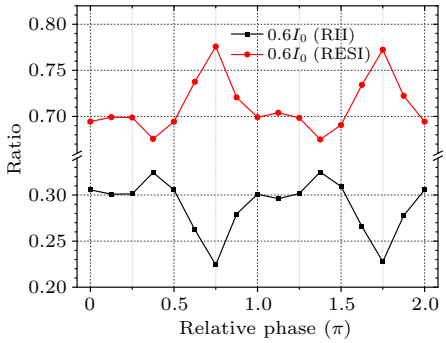


Fig. 6. The ratios of RESI and RII events to the total NSDI events are normalized and used as a function of relative phase. The laser field intensity is 0.6 PW·cm^{-2}. ($I_0 = 1$ PW·cm^{-2}).

Analyzing the subcycle dynamics of classical trajectories by tracing the evolution of trajectories that eventually lead to nonsequential double ionization is of great use in explaining the correlated momentum spectrum of the two electrons. As shown above, the absolute yield of the RESI channel is always much higher than that of the RII channel. Therefore, a typical relative phase (0.375π) is chosen in Fig. 6 to obtain a higher yield of the RII channel and thus avoid the risk that physical phenomena are not obvious due to the low yield of the RII channel. The electron–electron momentum correlation spectra of the two channels are shown in Fig. 7. In the RII channel, the momentum of the two electrons is strongly correlated, and the distributions in different subcycles are obviously different. This is strongly related to the fact that the delay time ($t_{\rm delay}$) in the RII channel is less than 0.2 cycles, which means that the second electron is ionized immediately after the recollision. Due to the shorter delay time, the electric field of the laser changes less, resulting in the two electrons being emitted in the same direction. As shown in Fig. 7(a), the blue histogram represents the probability distribution of the recollision time and the orange histogram represents the probability distribution of the NSDI time. During the period of 4–4.2 cycles, the momentum of the two electrons in the RII channel is distributed in the first quadrant. This is because the electric field of the laser is in the negative direction during the period from the recollision of the first electron with the parent ion to the ionization of the second electron, and the electrons are emitted in the direction of high potential. In the next window of double ionization time (4.2–4.4 cycles), the momentum distribution is electrons is mainly concentrated in the zero-coordinate region because the direction of the laser electric field corresponding to $t_{\rm delay}$ in this part has undergone a process from negative to positive. Unlike the RII channel, the momentum of the two electrons in the RESI channel does not exhibit a significant correlation phenomenon. Instead, it shows a cross-shaped distribution in the range of 4.4 to 5.2 cycles, as shown in Fig. 7(b). Let us take the uncorrelated phenomenon in the range of 4.4 to 4.6 cycles as an example. The time at which the first electron recollides with the parent core is in the lower range of 4 to 4.2 cycles or even earlier, while the transferred energy is insufficient to ionize the second electron directly. The second electron is emitted only after a longer relaxation time (> 0.2 cycles) in the subsequent optical field, during which the external field has already undergone significant change. Similarly, the same process occurs in the subsequent intervals of several optical cycles. The process described above is the reason why the momentum correlation between the two electrons in the RESI channel is not obvious.

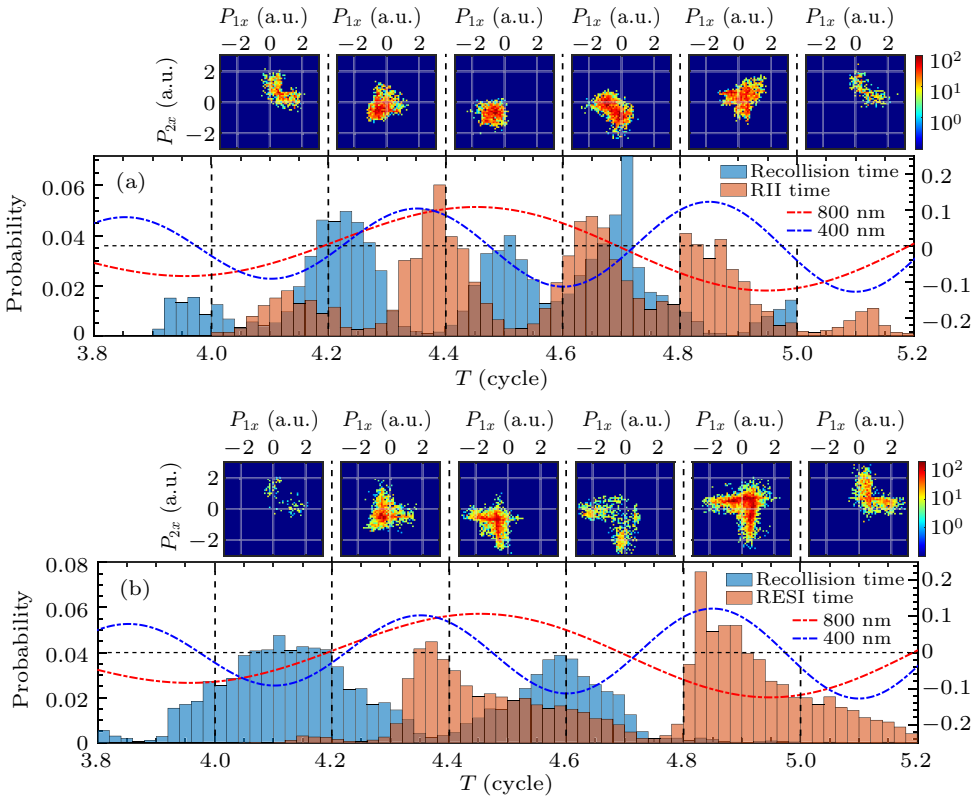


Fig. 7. The electron–electron momentum correlation spectra along the 800 nm laser polarization direction at the moment of NSDI, and the probability distribution of moment of recollision and NSDI in different optical cycles. The relative phase of laser fields in two spectra is 0.375π and the laser intensity is 0.6 PW·cm^{-2}: (a) RII events, (b) RESI events.

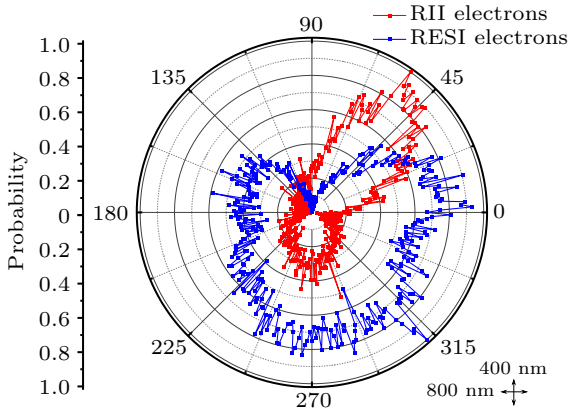


Fig. 8. The angle distribution of electrons at the moment of NSDI for the RII electrons (red line) and RESI electrons (blue line). The laser field intensity is 0.6 PW·cm^{-2}. The 0°–180° axis is the direction of polarization of the 800 nm laser, while the 90°–270° axis is along the direction of polarization of the 400 nm laser.

To verify the reliability of the above assumptions, the angular distribution of the emitted electrons in the two channels at the moment of NSDI (i.e., the moment of double ionization during the NSDI process) is shown in Fig. 8. For RII events (red line), the angle is mainly distributed in a narrow range from 40° to 60°, which means that the two electrons are more likely to be emitted in the same direction. For RESI events (blue line), the angle is distributed over an extremely wide range, which means that the two electrons are emitted in different directions without strong correlation. The difference in the angular distribution of electrons emitted from different channels can be used to verify that the OTC laser field can effectively control electron–electron momentum correlation in the 2D plane.

4. Conclusion and perspectives

In this work, we used the classical ensemble method to systematically study the NSDI process of Ar atoms driven by a few-cycle OTC laser field. The dependence of the NSDI process on the parameters of the OTC laser field was analyzed in detail. By regulating the relative phase and intensity of the laser field, we can optimize the yield and control the recollision time and travel time of the first electron on an attosecond time scale. Then, the information on the classical trajectory was analyzed and two different NSDI channels, RII and RESI, were determined. Finally, by analyzing the electron–electron momentum correlation at the moment of NSDI in different time windows and the angular distribution of the emitted electrons in different channels, it was found that the electron–electron correlation phenomenon is more obvious in the RII channel, which is due to the shorter delay time of the RII channel. Since the electrons can be controlled by the OTC laser field on a 2D plane before returning to the parent nucleus, observing electron–electron correlation based on the dynamic behavior of electrons in a strong field can be a powerful tool for studying ultrafast molecular dynamics and controlling photochemical reactions at the attosecond scale.

Acknowledgements

The work was partly supported by the National Natural Science Foundation of China (Grant Nos. 12034008, 12250003, and 11727810) and the Program of Introducing Talents of Discipline to Universities 111 Project (B12024).

References

[1] Strickland D and Mourou G 1985 *Opt. Commun.* **55** 447
[2] Zewail A H 1996 *J. Phys. Chem.* **100** 12701
[3] Corkum P B 1993 *Phys. Rev. Lett.* **71** 1994
[4] Uiberacker M, Uphues T, Schultze M, Verhoef A J, Yakovlev V, Kling M F, Rauschenberger J, Kabachnik N M, Schröder H, Lezius M, Kompa K L, Muller H G, Vrakking M J J, Hendel S, Kleineberg U, Heinzmann U, Drescher M and Krausz F 2007 *Nature* **446** 627
[5] Goulielmakis E, Loh Z H, Wirth A, Santra R, Rohringer N, Yakovlev V S, Zherebtsov S, Pfeifer T, Azzeer A M, Kling M F, Leone S R and Krausz F 2010 *Nature* **466** 739
[6] Mevel, Breger, Trainham, Petite, Agostini, Migus, Chambaret and Antonetti 1993 *Phys. Rev. Lett.* **70** 406
[7] Protopapas M, Keitel C H and Knight P L 1997 *Rep. Prog. Phys.* **60** 389
[8] Chen S G, Jiang W C, Grundmann S, Trinter F, Schöffler M S, Jahnke T, Dörner R, Liang H, Wang M X, Peng L Y and Gong Q 2020 *Phys. Rev. Lett.* **124** 043201
[9] Wang Y, Xu S, Quan W, Gong C, Lai X, Hu S, Liu M, Chen J and Liu X 2016 *Phys. Rev. A* **94** 053412
[10] Zhang L, Xie X, Roither S, Zhou Y, Lu P, Kartashov D, Schoeffler M, Shafir D, Corkum P B, Baltuska A, Staudte A and Kitzler M 2014 *Phys. Rev. Lett.* **112** 193002
[11] Ma X M, Zhou Y M, Chen Y B, Li M, Li Y, Zhang Q B and Lu P X 2019 *Opt. Express* **27** 1825
[12] Fu L B, Xin G G, Ye D F and Liu J 2012 *Phys. Rev. Lett.* **108** 103601
[13] Mancuso C A, Hickstein D D, Grychtol P, Knut R, Kfir O, Tong X M, Dollar F, Zusin D, Gopalakrishnan M, Gentry C, Turgut E, Ellis J L, Chen M C, Fleischer A, Cohen O, Kapteyn H C and Murnane M M 2015 *Phys. Rev. A* **91** 031402
[14] Moshammer R, Feuerstein B, Fischer D, Dorn A, Schroter C D, Deipenwisch J, Lopez-Urrutia J R C, Hohr C, Neumayer P and Ullrich J 2001 *Opt. Express* **8** 358
[15] Chen Z, Liang Y, Madison D H and Lin C D 2011 *Phys. Rev. A* **84** 023414
[16] Li S, Sierra-Costa D, Michie M J, Ben-Itzhak I and Dantus M 2020 *Communications Physics* **3** 35
[17] Lv W 2019 *J. Phys. B: Atom. Mol. Opt. Phys.* **52** 135601
[18] Xu J K, Li Y B, Zhou Y M, Chen Y K, Li M, Yu B H and Lu P X 2022 *Opt. Express* **30** 15951
[19] Huang C, Zhong M and Wu Z 2018 *Sci. Rep.* **8** 8772
[20] Xu T T, Zhang L L, Jin Z and Gong W J 2020 *Chin. Phys. B* **29** 093202
[21] Huang C, Zhong M and Wu Z 2019 *Opt. Express* **27** 7616
[22] Wei M, Kang H and Liu H 2024 *Opt. Express* **32** 2679
[23] Xu Q Y, Ben S, Sun Y, Xu H F, Liu X S, Lv H and Guo J 2020 *Chem. Phys. Lett.* **747** 137326
[24] Luo S Q, Ma X M, Xie H, Li M, Zhou Y M, Cao W and Lu P X 2018 *Opt. Express* **26** 13666
[25] Truong T, Anh-Tai T, Nguyen H, Nha N, Dung D and Pham V 2022 *Acta Physica Polonica, A.* **141** 569
[26] Song Q, Li H, Wang J, Lu P, Gong X, Ji Q, Lin K, Zhang W, Ma J, Li H, Zeng H, He F and Wu J 2018 *J. Phys. B: Atom. Mol. Opt. Phys.* **51** 074002
[27] Zhou Y, Liao Q, Zhang Q, Hong W and Lu P 2010 *Opt. Express* **18** 632
[28] Zhou Y, Huang C, Tong A, Liao Q and Lu P 2011 *Opt. Express* **19** 2301
[29] Li Y B, Qin L L, Liu A H, Zhang K, Tang Q B, Zhai C Y, Xu J K, Chen S, Yu B H and Chen J 2022 *Chin. Phys. Lett.* **39** 093201
[30] Gong X, Lin C, He F, Song Q, Lin K, Ji Q, Zhang W, Ma J, Lu P, Liu Y, Zeng H, Yang W and Wu J 2017 *Phys. Rev. Lett.* **118** 143203
[31] Xie X, Wang T, Yu S, Lai X, Roither S, Kartashov D, Baltuška A, Liu X, Staudte A and Kitzler M 2017 *Phys. Rev. Lett.* **119** 243201
[32] Wang X and Eberly J H 2012 *Phys. Rev. A* **86** 013421
[33] Haan S L, Smith Z S, Shomsky K N and Plantinga P W 2009 *J. Phys. B: Atom. Mol. Opt. Phys.* **42** 134009
[34] Yuan Z, Ye D, Xia Q, Liu J and Fu L 2015 *Phys. Rev. A* **91** 063417
[35] Zhou Y, Huang C, Liao Q and Lu P 2012 *Phys. Rev. Lett.* **109** 053004
[36] Talebpour A, Larochelle S and Chin S L 1997 *J. Phys. B: Atom. Mol. Opt. Phys.* **30** L245
[37] Walker B, Sheehy B, Dimauro L F, Agostini P, Schafer K J and Kulander K C 1994 *Phys. Rev. Lett.* **73** 1227